EARTHQUAKE ENGINEERING AND STRUCTURAL DYNAMICS
Earthquake Engng Struct. Dyn. 2015; **00**:1–18
Published online in Wiley InterScience (www.interscience.wiley.com). DOI: 10.1002/eqe

Shake Table Testing of an Elevator System in a Full-Scale Five-Story Building

Xiang Wang[1], Tara C. Hutchinson[1*†], Rodrigo Astroza[2], Joel P. Conte[1],
José I. Restrepo[1], Matthew S. Hoehler[3], and Waldir Ribeiro[4]

[1]*Department of Structural Engineering, University of California at San Diego, La Jolla, CA 92093*
[2]*Facultad de Ingenieria y Ciencias Aplicadas, Universidad de los Andes, Santiago, Chile*
[3]*National Institute of Standards and Technology, Gaithersburg, MD, 20899; formerly with Hilti Corporation*
[4]*Schindler Elevator Corporation, Randolph, NJ 07869*

SUMMARY

This paper investigates the seismic performance of a functional traction elevator as part of a full-scale five-story building shake table test program. The test building was subjected to a suite of earthquake input motions of increasing intensity, first while the building was isolated at its base, and subsequently while it was fixed to the shake table platen. In addition, low-amplitude white noise base excitation tests were conducted while the elevator system was placed in three different configurations, namely, by varying the vertical location of its cabin and counterweight, to study the acceleration amplifications of the elevator components due to dynamic excitations. During the earthquake tests, detailed observation of the physical damage and operability of the elevator as well as its measured response are reported. Although the cabin and counterweight sustained large accelerations due to impact during these tests, the use of well-restrained guide shoes demonstrated its effectiveness in preventing the cabin and counterweight from derailment during high-intensity earthquake shaking. However, differential displacements induced by the building imposed undesirable distortion of the elevator components and their surrounding support structure, which caused damage and inoperability of the elevator doors. It is recommended that these aspects be explicitly considered in elevator seismic design.

Received . . .

1. INTRODUCTION

Elevators are a common vertical transportation system and an important means of safe emergency egress in buildings. They are particularly important in high-rise buildings and essential facilities, such as hospitals, where emergency egress can be impaired due to the long egress distances or occupant immobility. Therefore, it is critical that elevators remain operable following an earthquake or other disasters [1, 2]. Depending on the type of hoist mechanisms, elevators can be classified into one of two major categories: 1) hydraulic elevators, or 2) traction elevators. Hydraulic elevators utilize a fluid pumping system to lift the cabin and usually do not have counterweights, and they are typically used in low to medium-rise buildings due to limitations on speed and travel distance. In contrast, traction elevators consist of a cabin attached to one end of hoist ropes and a counterweight attached to the opposite end to balance the cabin weight. Since the vertical movement of traction

*Correspondence to: Tara C. Hutchinson, Department of Structural Engineering, University of California at San Diego, La Jolla, CA 92093
†E-mail:tara@ucsd.edu

elevators is controlled by the hoist ropes passing through a motor-driven traction sheave, they are applicable to a broader range of buildings, in particular high-rise buildings.

Design and installation of elevators in the United States are governed by ASME A17.1 provisions [3]. Importantly, elevator guide-rails are attached to buildings at multiple supports along the height of the building, subjecting the elevator system to multiple-support excitations imposed by the building (e.g., interstory drifts, multiple-support accelerations). ASME A17.1 [3] recognizes the potential for seismic load and deformation transfer to the elevator and its components and therefore provides seismic design guidelines for elevator guide-rail systems. The design guidelines require that the stresses imposed on the guide-rails remain in the elastic range when subjected to seismic impact loading of the cabin and counterweight. In addition, deflections of the guide-rails and their attachment points need to be restricted within specified limits to prevent cabins and counterweights from derailment.

Although fatalities of elevator passengers have been extremely rare during past earthquakes, damage to elevator systems has often hindered building operability and emergency response efforts even following moderate intensity earthquakes (e.g., [4–7]). Traction elevators appeared to be more vulnerable to seismic damage than hydraulic elevators due to the presence of counterweights. Counterweight derailment (Figure 1a) has accounted for the most prominent damage in past earthquakes largely as a result of excessive impact loading imposed on the supporting guide-rail systems. Other common types of damage included bent guide-rails, guide-rail anchorage failure, collision of counterweights and cabins, machine-drive anchorage failure, jumped or twisted ropes, and falling counterweight blocks (Figure 1b).

(a)

(b)

Figure 1. Damage to elevators in Curanilahue hospital in Chile during the 2010 Maule earthquake (M_w = 8.8): (a) derailed counterweight, and (b) fallen counterweight blocks arrayed on the top of the cabin.

Analytical studies of the seismic behavior of elevators have been conducted previously [8–12], however, experimental validation of these computational models has been hampered by limited experimental data regarding the seismic performance of these systems. To the authors' knowledge, shake table testing of full-scale guide rail-counterweight subassemblies conducted in Taiwan [13] is the only experimental investigation on elevator systems to date. To expand the experimental database, a landmark full-scale five-story reinforced concrete building, outfitted with a broad array of nonstructural components and systems, was tested on the Large High-Performance Outdoor Shake Table [14] at the University of California, San Diego (UCSD) [15–17]. Within this test building, a fully functional traction elevator was incorporated at full-scale, allowing investigation of system-level interactions between the building and the elevator as well as interactions between individual components of the elevator. In this paper, the dynamic amplification characteristics of

DOI: 10.1002/eqe

the elevator are investigated using the white noise test data. In addition, observations and measured response of the elevator in the seismic tests are discussed, with particular emphasis on associating these responses with the seismic demands of the test building.

2. SHAKE TABLE TEST PROGRAM

The test building consisted of a cast-in-place five-story reinforced concrete structure with moment-resisting frames providing lateral resistance in the direction of shaking (east-west direction) (Figure 2a). The design utilized ground motions developed for a site in Southern California, with the maximum considered earthquake (MCE) ground motion spectrum for a Site Class D (stiff) soil conditions, with a short-period spectral acceleration S_{MS} = 2.1 g and a one-second spectral acceleration S_{M1} = 1.4 g. The MCE level performance targets of 2.5 % peak interstory drift ratio and a peak floor acceleration between 0.7 g and 0.8 g were selected during the conceptual design phase. As shown in Figure 2b, the building consisted of two bays in the longitudinal direction and one bay in the transverse direction, with a plan dimension of 11.0 m × 6.6 m. Two moment resisting frames were placed in the east bays in the longitudinal (shaking) direction, while two shear walls were placed within the interior the building to resist transverse lateral and partial torsional loads. The floors were constructed of cast-in-place concrete and incorporated two large openings, one on the northwest to facilitate a full-height elevator shaft and the other on the southeast to accommodate the stairs. The building floor-to-floor height was 4.3 m at each level, resulting in a total building height of 21.3 m above the foundation (Figure 2c). The building (excluding the foundation) had an estimated weight of 3010 kN for the structural skeleton and a total weight of 4492 kN including all nonstructural components and systems, and the foundation had an estimated weight of 1868 kN.

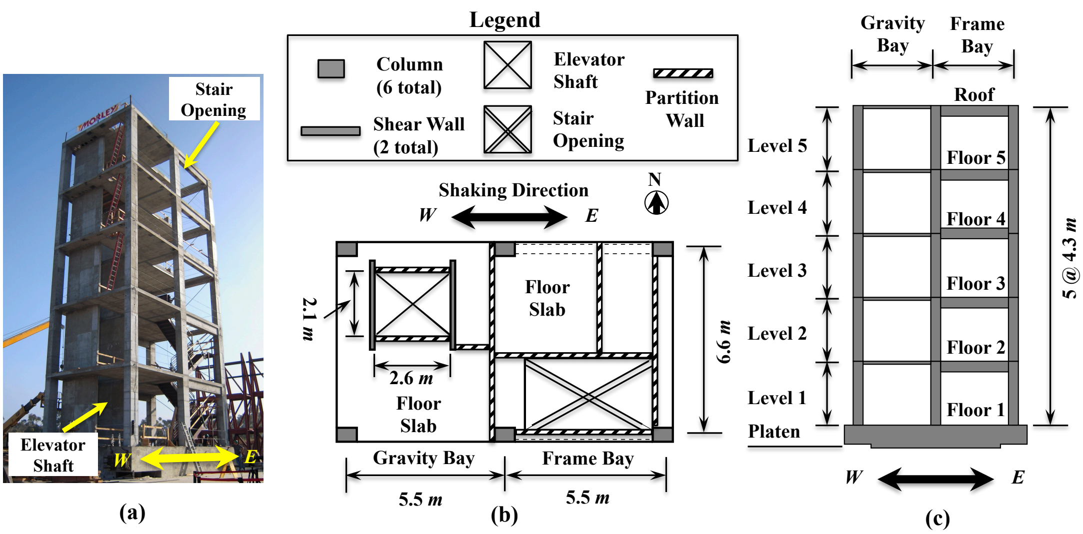

Figure 2. Test building: (a) photograph of structural skeleton, (b) plan layout (level 3), and (c) elevation (shear walls not shown in part (c) for clarity).

The seismic test program was comprised of two test phases, namely: (i) the building isolated at its base (BI) and subjected to seven earthquake input motions, and (ii) the building fixed at its base (FB) and subjected to six earthquake input motions. In addition, low-amplitude white noise base excitation tests were conducted at various stages during the test program to facilitate identification of the dynamic characteristics of the test building and its nonstructural components and systems. All earthquake and white noise test motions were applied in the east-west direction using the single-axis shake table, whose axis coincided with the longitudinal axis of the building. The earthquake input motions and measured building peak responses are summarized in Table I.

DOI: 10.1002/eqe

This table also summarizes the peak floor accelerations (PFAs) at the roof and the peak interstory drift ratios (PIDRs) at level 2, which represent the largest peak responses of the building during each test. It is also noted that although the building fundamental period T_1 varied during the testing due to accumulated structural damage, dominant period values of 2.5 s for the building in the base isolated test phase and 1.0 s for the fixed base test phase are used for evaluating the elastic spectral accelerations at the building fundamental period $S_a(T_1,\xi)$.

Table I. Summary of earthquake input motions and measured building peak responses.

Test phase	Motion name	PIA^1 (g)	PIV^2 (m/s)	PID^3 (m)	$S_a(T_1,\xi)^4$ (g)	$PFA_R{}^5$ (g)	$PIDR_{L2}{}^6$ (%)	Elevator test configuration[7]
Base isolated (BI)	BI-1:CNP100	0.21	0.23	0.08	0.09	0.09	0.08	C-I
	BI-2:LAC100	0.22	0.24	0.09	0.06	0.10	0.10	C-I
	BI-3:LAC100	0.25	0.24	0.09	0.08	0.10	0.11	C-III
	BI-4:SP100	0.52	0.35	0.08	0.08	0.12	0.10	C-III
	BI-5:ICA50	0.17	0.22	0.04	0.08	0.08	0.09	C-I
	BI-6:ICA100	0.31	0.43	0.09	0.15	0.16	0.19	C-I
	BI-7:ICA140	0.50	0.63	0.13	0.23	0.26	0.32	C-I
Fixed base (FB)	FB-1:CNP100	0.21	0.24	0.09	0.33	0.44	0.47	C-I
	FB-2:LAC100	0.18	0.23	0.09	0.29	0.39	0.56	C-I
	FB-3:ICA50	0.21	0.26	0.06	0.47	0.58	0.94	C-I
	FB-4:ICA100	0.26	0.28	0.07	0.46	0.64	1.41	C-I
	FB-5:DEN67	0.64	0.64	0.20	1.13	0.99	2.75	C-I
	FB-6:DEN100	0.80	0.84	0.34	1.36	0.90	5.99	C-I

[1] PIA – peak input acceleration (achieved); [2] PIV – peak input velocity (achieved); [3] PID – peak input displacement (achieved) ; [4] $S_a(T_1,\xi)$ – elastic spectral accelerations of the input motion (T_1 = 2.5 s and ξ = 12% for the base-isolated building, T_1 = 1.0 s and ξ = 5% for the fixed-base building); [5] PFA_R – (averaged) peak floor acceleration at the roof; [6] $PIDR_{L2}$ – (averaged) peak interstory drift acceleration at level 2; [7] Detail discussions of elevator test configurations are presented in Section 3.4.

As the seismic demands on the building (superstructure) were relatively low during the base isolated test phase (with PIDR < 0.4 % and PFA < 0.3 g), the building sustained only minor damage to its nonstructural components (e.g., partition walls [18]) and very little damage to its structure [15]. During the fixed base test phase, the earthquake motions were applied with increasing intensity to progressively damage the structure. Figure 3 presents the peak building responses (PFA and PIDR) during the fixed base test phase. It is noted that the design target PIDR of about 2.5 % was achieved during test FB-5, while well above the design target PIDR of 6 % was attained during test FB-6. As a result of the large interstory drift demands, the building was severely damaged during the last two fixed base tests. Physical damage during test FB-6 included fracture of the longitudinal reinforcement within the frame beams and partial development of punching shear mechanisms at the slab-column interfaces of the second and third floors, as a result of formation of intermediate mechanism of the building. Additional information regarding the broader test program and key results of the shake table test program is available in [15, 19].

3. ELEVATOR SYSTEM

3.1. Specimen Description

A fully functional traction elevator was installed to access all levels of the building (except the roof) at the northwest side of the test building (Figure 2a). As shown in Figure 4a–b, the shaft had a dimension of 2.6 m × 2.1 m and was enclosed by reinforced concrete shear walls on the east and west faces and cold-formed steel partition walls on the south and north faces. The cabin was located in the middle of the hoistway, while the counterweight was located on the east side. The brackets on the east wall (Omega brackets) provided support for three guide-rails (one for the cabin and two for the counterweight), while the brackets on the west wall (Z bracket) supported the single cabin

DOI: 10.1002/eqe

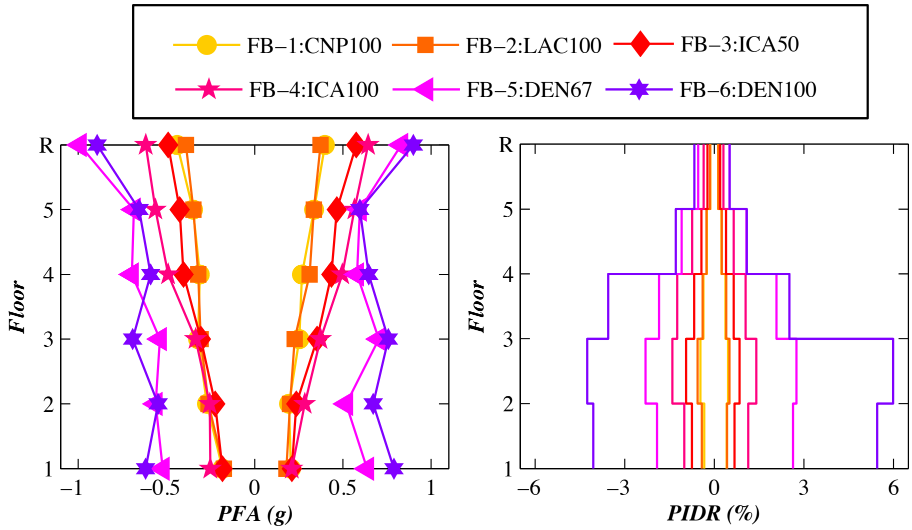

Figure 3. Building peak response during the fixed base (FB) test phase: (a) peak floor acceleration (PFA), and (b) peak interstory drift ratio (PIDR).

guide-rail. The drive machine and the sheave were located on top of the guide-rails on the east side of the shaft. Details of the key elevator components are described as follows:

- *Cabin*: the interior dimensions of the cabin were 2.1 m × 1.7 m × 2.4 m and the weight was ~9.4 kN. Sand bags weighting 6.2 kN (40 % of the elevator's rated capacity) were placed inside of the cabin during all seismic tests and white-noise excitation tests to simulate a passenger load, resulting in a total weight of ~15.6 kN.
- *Counterweight*: the dimensions of the counterweight frame were 2.7 m × 1.2 m and its total weight (including the steel plates) was ~16.0 kN (Figure 4e).
- *Guide-rails*: 18.0 kg/m guide-rails were used for the cabin, whereas the counterweight utilized 12.3 kg/m guide-rails.
- *Brackets and anchorage*: Omega brackets (Figure 4c) and Z bracket (Figure 4d) were evenly spaced along the vertical direction of the shaft walls at an interval of ~2.1 m (half the story height). With the exception of the brackets at floor 4 that each employed two M16 T-headed bolts attaching to cast-in anchor channels, all brackets were attached to the shaft walls with two M16×120 mm bolt-type expansion (wedge) anchors on each bracket. The attachment locations of the bracket anchors are shown in Figure 4c–d.
- *Doors*: the elevator doors were located at the south side of the shaft at all levels, each with an opening of 2.1 m in height and 1.1 m in width. The door frame was made of 1.2 mm thick stainless steel hollow section, with a cross-section dimension of 120 mm × 180 mm. As shown in Figure 4f, the door frame was enclosed within the surrounding cold-formed steel shaft walls, which had a stud thickness of 250 mm and stud spacing at ~0.6 m on center (detailed description of the cold-formed steel shaft walls are available in [18]). As such, the door and the shaft wall at each level were subjected to the building interstory drift demands.
- *Guide shoes*: both the cabin and counterweight adopted guide shoes for restraining the horizontal movement of the components (Figure 4g). The gap width between the T-shape guide-rails and the guide shoes was limited to 1.5 mm at the two sides of guide-rails and 5 mm at the tip of the guide-rails.

3.2. Elevator Design

The elevator in the test building was designed in accordance with ASME A17.1 provisions [3]. The required deflection of the bracket support (attachment point of bracket anchors on the shaft

DOI: 10.1002/eqe

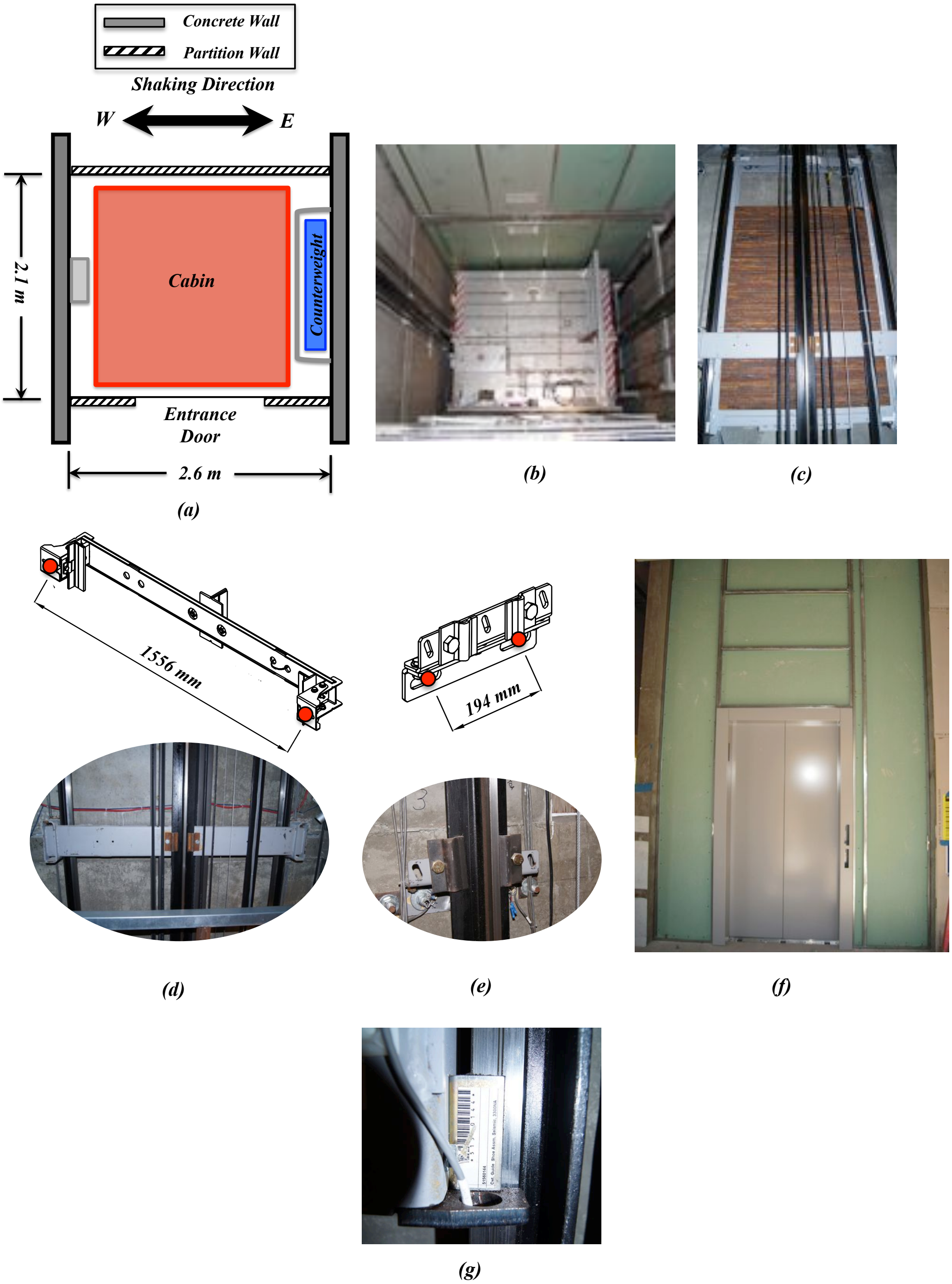

Figure 4. Elevator hoistway and component details (a) schematic plan layout of the hoistway, (b) the hoistway viewing down from level 3, (c) Omega bracket, (d) Z bracket, (e) counterweight, (f) elevator door and surrounding cold-formed steel shaft wall, and (g) counterweight guide shoe (red dots in parts (c) and (d) indicate the attachment locations of bracket anchors).

walls) was limited to 2.5 mm, and the total deflection of the rail support (including the bracket and the building support deflection) was limited to 6 mm. Two lateral load cases – non-seismic (normal operation) and seismic – were considered in the strength design of the guide-rail systems.

DOI: 10.1002/eqe

For non-seismic applications, the horizontal loads were the maximum static loads based on the cabin and counterweight guide shoes reaction loads during its normal operation as recommended by the manufacturer. For the seismic design, however, horizontal forces applied on the guide-rail system were determined as the seismic impact loads of the cabin and counterweight in addition to the inertial forces induced by the machine drive and its support on top of the guide-rails. Horizontal accelerations of 0.5 g for the cabin and counterweight and 1.0 g for the machine drive and its support were considered in the seismic design.

3.3. Instrumentation

The response of the building structure was monitored with a dense accelerometer array that was connected to a standalone data acquisition system sampling data at a frequency of 200 Hz. The building accelerations at each floor were measured using four tri-axial accelerometers installed at the four corners of the floor. The floor displacements of the building were obtained by double integrating the measured floor accelerations, and the roof displacements determined using the double integration method were verified by independent differential Global Positioning Satellite (GPS) measurements. The interstory drift ratios of the building were subsequently calculated as the difference of two averaged displacement histories between sequential floors normalized by the floor height. While the uncertainty of the measured accelerations was relatively low (with an estimated expanded uncertainty of ±0.002 g), the reported building floor displacements (or interstory drifts) were subjected to larger uncertainties since they were double integrated using the acceleration measurements. The relative error of the PIDR measurements could be within the range of 5% and 10%, depending on the level of building nonlinearity during the earthquake tests [20]. The measured building structural responses (e.g., PFA and PIDR as presented in Figure 3) are considered as system-level input for the elevator system.

The elevator was instrumented with an array of uni-axial accelerometers deployed on the cabin and the counterweight as well as strain gauges embedded within the bracket anchors at select locations. These sensors were all connected to a multi-node distributed data acquisition system, which collected data at a sampling frequency of 240 Hz. As shown in Figure 5a–b, six uni-axial accelerometers were installed on each of the cabin (CAB-X-X) and counterweight (CWT-X-X) to measure the acceleration response of these components and their amplification effects relative to the floor excitations. In addition, all bracket anchors at floor 1 and from floor 4 to the mid-height of level 5 were instrumented with uni-axial strain gages (SG-X-X) installed concentrically in the anchor shaft between the nut and the anchor expansion cone (Figure 5c). This resulted in a total of twenty instrumented anchors, since each bracket consisted of a pair of anchors attached to it (distinguished by SG-X-XS and SG-X-XN). Each instrumented anchor was calibrated prior to installation to establish the relation between the axial strain and applied axial load, and the expanded uncertainty of the force measurements was estimated as ±0.2 kN. These instrumented anchors measured the axial anchor forces induced by either impacts between the elevator components and the guide-rails or differential displacements at multiple guide-rail bracket supports. Shear forces in the anchors were not measured because the primary loading direction was parallel to the anchor longitudinal axis. It is noted that the instrumented wedge anchors were initially installed with the required installation torque of 81 N-m to set the anchor expansion elements in the drilled holes and clamp the guide-rail brackets in position. The pretension was subsequently removed and set to 5 N-m to effectively eliminate the clamping force, thus allowing the strain gauges to measure the seismically induced anchor tension forces. The cast-in anchor channel T-headed bolts were installed with the required installation torque of 200 N-m, which was retained during the earthquake tests to assure proper function of these anchors. Therefore, the force measurements in these bolts are expected to be insignificantly small (<< 1kN) unless the clamping force is exceeded by earthquake induced tension forces in these bolts. Additional details of the instrumentation of the test building and the elevator can be found in [21].

DOI: 10.1002/eqe

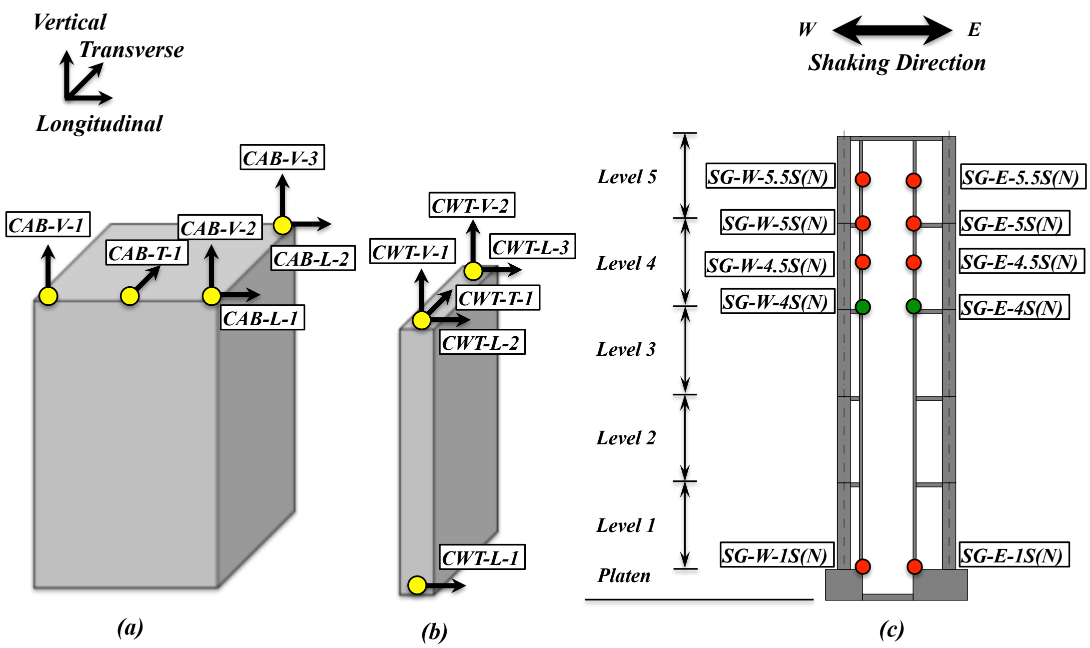

Figure 5. Elevator instrumentation: (a) accelerometers on the cabin, (b) accelerometers on the counterweight, and (c) strain gauges of the bracket anchors (SG-X-XS and SG-X-XN denote the anchor on the north or south side attaching the same bracket).

3.4. Test Configurations

As shown schematically in Figure 6a, three test configurations were considered by varying the location of the cabin and the counterweight in the white noise (WN) tests: a) configuration C-I – the cabin at level 1 and the counterweight at level 5; b) configuration C-II – both the cabin and the counterweight at the building mid-height (level 3); and c) configuration C-III – the cabin at level 5 and the counterweight at the level 1. It is noted that an elevator is expected to spend the majority of its life cycle in Configuration I, and, therefore, this configuration was adopted as the primary configuration in the seismic tests (Table I). For C-I, the acceleration responses at floor 1 may be considered as input to the cabin and those at floor 5 may be considered as input to the counterweight; likewise, the acceleration responses at floor 5 may be considered as input to the cabin and those at floor 1 may be considered as input to the counterweight for C-III. When the cabin and the counterweight are concentrated at level 3 (C-II), the acceleration responses at floor 3 impose the predominant demand on these components.

The mass of the elevator components (cabin and counterweight) was significantly smaller than that of the corresponding floor of the building. With the largest concentration of elevator mass in configuration C-II, the mass of the cabin and counterweight combined was less than 5 % of the mass of the corresponding floor. As a result, the modal frequencies of the building remained nearly identical regardless of the location of the cabin and counterweight. As shown in Figure 6b, the identified frequencies of the first three vibrational modes of the test building under the RMS 1.5 % g WN tests – the first longitudinal (1-L) mode, the first transverse and torsional (1-T+To) mode, and the first torsional (1-To) mode – varied by less than 5 % under the three test configurations [22]. It is noted that the elevator-building mass ratio may be even smaller for typical buildings, as the test building had a small footprint compared with buildings used in practice. This fact may lead to the conclusion that the impact of the elevator on the fundamental frequencies of the building would be even less.

DOI: 10.1002/eqe

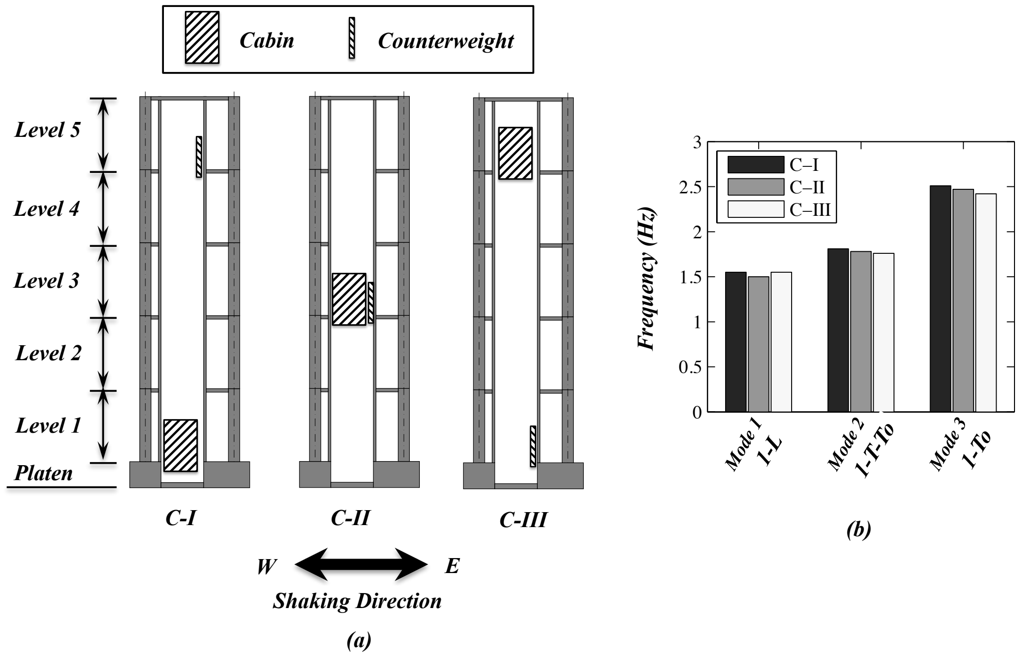

Figure 6. (a) Test configurations for the elevator system (west bay of the building), and (b) the identified modal frequencies of the building associated with different test configurations.

4. WHITE NOISE TEST RESULTS

Low-amplitude white noise base excitation tests, while the elevator was placed in each of the three test configurations, were conducted prior to the seismic tests, while the building was fixed at its base. The primary objective of the white noise tests was to study the dynamic acceleration amplification characteristics of the elevator cabin and counterweight under the three different test configurations. It is noted that the elevator was operational and the installation of nonstructural components within the test building was nearly complete. Under each of the three test configurations, the white noise tests consisted of input excitations of two distinct amplitude levels with nominal (target) root-mean-square (RMS) accelerations of: 1.0 % g and 1.5 % g. It is noted, however, that the amplitude of the achieved excitation in the first RMS 1.0 % g white noise test (C-I) was twice as large as the other two tests with identical target amplitudes, and therefore the results from this test are not included in the study.

Table II summarizes the peak component accelerations (PCAs) of the cabin and counterweight and the associated peak floor accelerations (PFAs) measured during the white noise tests. The acceleration amplification ratios of the elevator components Ω, defined as the ratio between the PCA of individual components (cabin and counterweight) and the PFA of the associated floor, are also presented in the table. The measured acceleration responses were filtered with a fourth-order Butterworth filter with band-pass frequencies between 0.25 Hz and 100 Hz to preserve the high-amplitude impulse-like acceleration responses. As shown in the table, the amplification effects of the counterweight were notably larger compared with those of the cabin at similar locations. The acceleration amplification effects of the cabin were significant ($\Omega > 3.5$) only when the cabin was located at the top (C-III) but remained moderate in the other two configurations ($\Omega < 2$). In contrast, the amplification ratio Ω exceeded 4 when the counterweight was at the top of the building (C-I) and reached as much as 7 when the counterweight was located at the mid-height of the building (C-II). Since the masses of the cabin and counterweight were comparable in these tests, the differences in the acceleration amplification effects between the cabin and the counterweight may be attributed to

Prepared using eqeauth.cls
DOI: 10.1002/eqe

Table II. Acceleration responses of the cabin and counterweight in the white noise tests.

Test configuration	RMS amplitude		Cabin			Counterweight		
	Target (g)	Achieved (g)	PFA (g)	PCA^{cab}_{long} (g)	Ω^{cab}_{long}	PFA (g)	PCA^{cwt}_{long} (g)	Ω^{cwt}_{long}
C-I	1.5 %	0.93 %	0.07	0.08	1.13	0.09	0.45	4.92
C-II	1.0 %	0.62 %	0.02	0.03	1.42	0.02	0.15	6.90
	1.5 %	0.85 %	0.06	0.10	1.80	0.06	0.30	5.13
C-III	1.0 %	0.56%	0.03	0.17	5.56	0.02	0.04	1.94
	1.5 %	0.84 %	0.09	0.31	3.51	0.06	0.17	2.59

Notes: PFA = peak floor acceleration associated with either the cabin and or counterweight (as relevant); PCA^{cab}_{long}, PCA^{cwt}_{long} = peak component accelerations of the cabin and counterweight in the longitudinal direction; Ω^{cab}_{long}, Ω^{cwt}_{long} = acceleration amplification factor of the cabin and counterweight in the longitudinal direction.

the detailing and varied flexibility of the guide-rails (e.g., guide-rail section dimensions, attachment details, gap provisions).

5. EARTHQUAKE TEST RESULTS

5.1. Physical Observations

Post-shaking inspection of the elevator was conducted at each inspection phase immediately following the seismic test to characterize the physical damage of individual components and to evaluate its functionality. The inspections were conducted by operating the elevator along the full height of the building and performing stops at each floor. The elevator remained fully operational and no damage to the elevator was observed up through test FB-4. The onset of damage was first observed following test FB-5 (design event earthquake with a PIDR of 2.5 % at level 2) in the form of incipient door gaps (<25 mm) and minor crushing of the door with the surrounding cold-formed steel partition walls at levels 2 and 3 of the building (Figure 7a). The elevator remained functional in spite of the presence of these gaps. During test FB-6, however, the doors at the lower three levels sustained severe damage when averaged PIDR demands were extremely large (~6 % at the lower two levels and ~3.5 % at level 3). The gaps between the doors at levels 2 and 3 reached a maximum

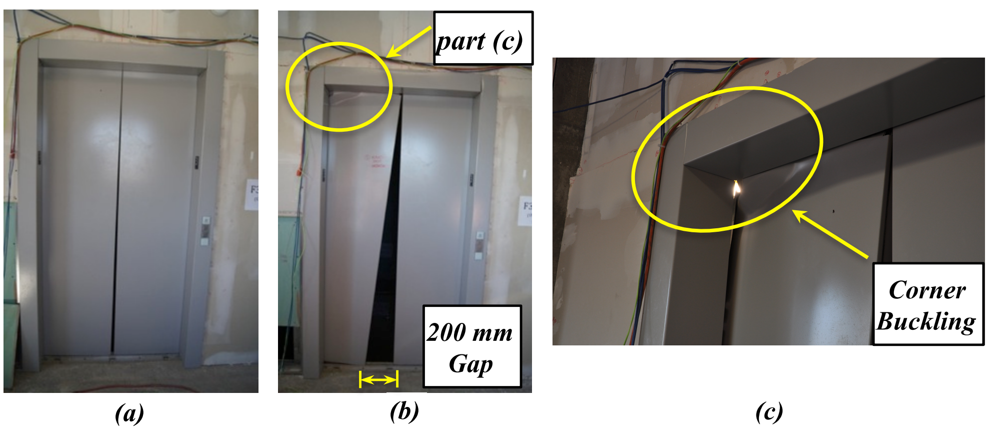

Figure 7. Damage to the elevator: (a) incipient gapping of the door at level 3 following test FB-5, (b) door distortion at level 3 following test FB-6, and (c) corner crushing of the door at level 3 following test FB-6.

DOI: 10.1002/eqe

residual of 200 mm at their base (Figure 7b), and corner crushing of the elevator doors progressed as a result of severe interaction between the doors and the partition walls (Figure 7c). The damaged doors eventually resulted in inoperability of the elevator and loss of compartmentation in the case of post-earthquake fire [23]. However, inspection conducted during the demolition stage revealed no visible damage to the cabin, the counterweight, the guide-rail and anchorage system, or other components within the elevator shaft. Elastic flexing of the guide rails in the vertical direction was detected, possibly due to the residual drifts of the building at the end of the tests.

5.2. *Measured Response*

5.2.1. Accelerations. The absolute acceleration time histories of the cabin and counterweight during test FB-1 (elevator in configuration C-I) and the associated Fourier amplitude spectra are presented in Figure 8. The longitudinal accelerations of the cabin (CAB-L-1 and CAB-L-2) and counterweight (CWT-L-2 and CWT-L-3) were comparable at the two corners of each component, however the counterweight accelerations contained much more high-amplitude impulse-like contents in their responses. Since no transverse excitation was imposed on the test building, the transverse floor excitations and the transverse accelerations of the cabin and counterweight (CAB-T-1 and CWT-T-1) were much smaller than their longitudinal counterparts, and the individual

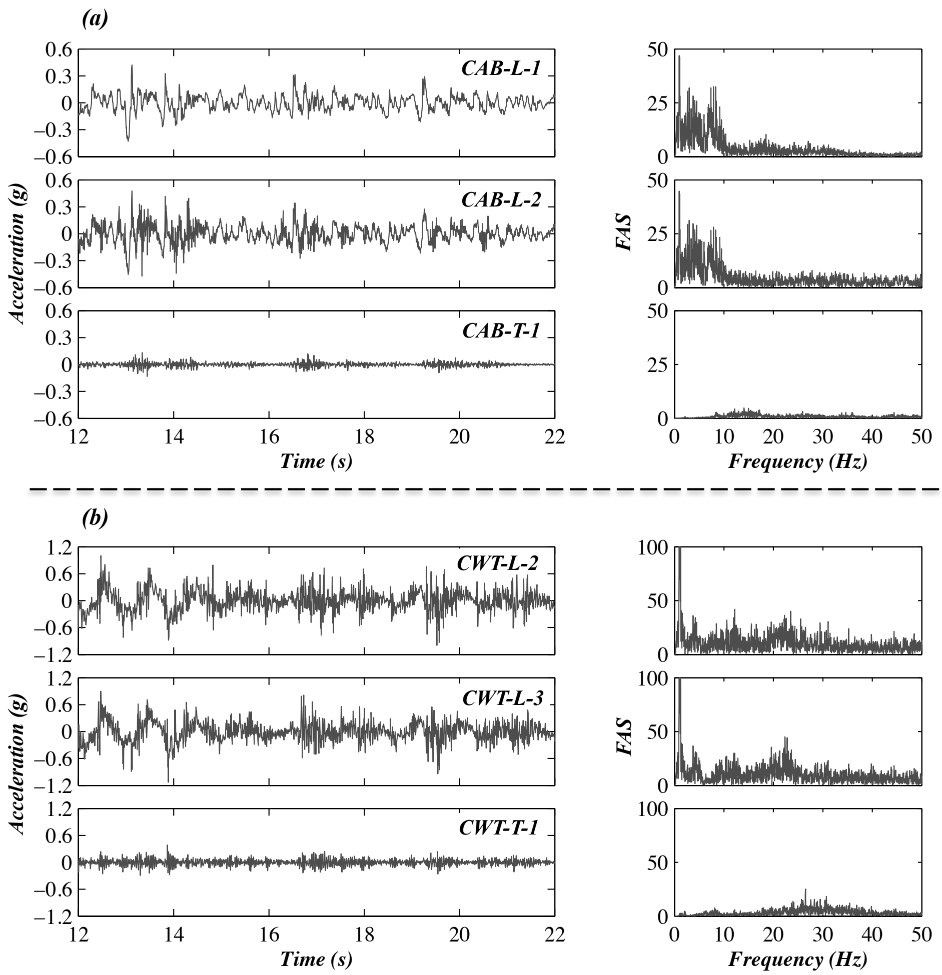

Figure 8. Acceleration time histories and associated Fourier amplitude spectrum (FAS) of: (a) cabin, and (b) counterweight during test FB-1 (with a high frequency cutoff of 100 Hz).

DOI: 10.1002/eqe

peaks of the transverse acceleration responses coincided with the impulse-like responses in the longitudinal direction. The Fourier amplitude spectra of the acceleration responses indicate that the longitudinal accelerations of the cabin and counterweight were dominated by responses with frequencies less than 10 Hz, and the peaks consistently occurred around 1 Hz, which corresponds to the first longitudinal vibration mode of the test building. In contrast, the transverse accelerations contained frequency contents primarily higher than 10 Hz, possibly associated with their individual natural frequencies excited by the impact loading.

Table III summarizes the peak component accelerations (PCAs) of the cabin and counterweight and their associated longitudinal peak floor accelerations (PFAs) during all seismic tests. It is noted that two band-pass Butterworth filters with different high frequency cutoff values were applied on the measured acceleration histories. The first filter, with a high frequency cutoff of 100 Hz (Nyquist frequency of the measured data), is intended to preserve high-amplitude impulse-like responses recorded on individual components due to impact loading, as these responses may damage the electronic components of the elevator. However, these impulse-like responses may involve high-frequency local vibration as opposed to global acceleration responses of the elevator components, and therefore a second filter with a high frequency cutoff of 25 Hz was applied to remove these high frequency impulses. For each application, the low frequency cutoff was selected as 0.25 Hz. During the base isolated tests, the longitudinal PCAs of the cabin and the counterweight were relatively low (0.25 g for the cabin and 0.4 g for the counterweight) when the impulse-like responses were included and even lower (0.2 g for the cabin and 0.3 g for the counterweight) when the impulse-like responses were filtered. As the associated PFAs became slightly larger during the first four fixed base tests, the observed PCAs of the cabin increased moderately (to about 0.6 g), and those of the counterweight increased sharply (as large as 1.8 g). During the last two fixed base tests (FB-5 and FB-6), extremely large impulse-like accelerations (>6 g) were measured on both the cabin and counterweight as a result of the pronounced increase of the input excitations. By applying the filter with the 25 Hz high frequency cutoff these acceleration responses remained larger than 3 g for the cabin and counterweight. The transverse PCAs of the cabin were significantly lower than their longitudinal counterparts in both the base isolated and fixed base test phases (<0.6 g). However, while the transverse PCAs of the counterweight were also much lower than their longitudinal counterparts in the base isolated tests and the first four fixed base tests, the peak accelerations became very large in the last two fixed base tests, with amplitudes as large as 1/3 of those in the longitudinal direction. Provided the fact that no input excitation was applied in the transverse direction and the building torsional response was not significant, these large transverse accelerations were possibly due to the oblique impact between the counterweight and the guide-rails.

Figure 9 presents the acceleration amplification ratios the cabin and counterweight compared with the associated PFAs in the seismic tests. The acceleration amplification ratio Ω is determined as the ratio between the PCA of the individual component and the PFA of the associated floor. As the PFAs of the cabin and counterweight were comparable during the base isolated tests, the cabin observed only slight acceleration amplification effects ($\Omega < 1.5$), but the amplification effects were larger for the counterweight ($\Omega = 1.5 - 3$) (Figures 9a and 9b). The amplification effects continued to increase during the first four fixed base tests as the associated PFAs became higher; Ω was as large as 3 for the cabin and 4 for the counterweight while the impulse-like acceleration responses were preserved (Figure 9c and 9d). As both the cabin and counterweight sustained significant impacts during the last two fixed base tests, Ω increased sharply and attained values as large as 7 for the cabin and 9 for the counterweight when the high cutoff frequency is selected as 100 Hz and about 5 when it is selected as 25 Hz. It is noted that the observed acceleration amplification ratios of both the cabin and counterweight during the FB tests were much larger than those prescribed in Table 13.6-1 of ASCE 7-10 [24], in which the acceleration amplification factor a_p is defined as 1.0 for elevator components, assuming them as rigid nonstructural components. Although no observable damage to the elevator components was directly attributed to these high acceleration amplification effects, it is recommended that future investigation be conducted to provide design guidelines regarding expected peak accelerations of elevator components during earthquakes.

DOI: 10.1002/eqe

Table III. Peak component acceleration responses of the cabin and counterweight during the seismic tests (units of g).

Test name	Cabin							Counterweight						
	PFA	CAB-L-1		CAB-L-2		CAB-T-1		PFA	CWT-L-2		CWT-L-3		CWT-T-1	
		100 Hz$^+$	25 Hz$^+$	100 Hz	25 Hz	100 Hz	25 Hz		100 Hz	25 Hz	100 Hz	25 Hz	100 Hz	25 Hz
BI-1	0.08	0.09	0.09	0.11	0.08	0.01	0.01	0.01	0.27	0.16	0.21	0.13	0.07	0.03
BI-2	0.09	0.10	0.10	0.10	0.09	0.01	0.01	0.09	0.34	0.17	0.25	0.20	0.07	0.03
BI-3*	0.10	0.10	0.10	0.10	0.10	0.01	0.01	0.09	0.20	0.16	0.15	0.12	0.07	0.03
BI-4*	0.10	0.12	0.12	0.12	0.11	0.02	0.02	0.10	0.28	0.22	0.23	0.18	0.13	0.04
BI-5	0.07	0.08	0.08	0.08	0.08	0.01	0.01	0.08	0.24	0.15	0.19	0.15	0.05	0.03
BI-6	0.14	0.15	0.15	0.15	0.14	0.01	0.01	0.15	0.27	0.19	0.26	0.22	0.07	0.04
BI-7	0.18	0.23	0.21	0.21	0.20	0.02	0.01	0.24	0.44	0.28	0.41	0.30	0.13	0.05
FB-1	0.21	0.43	0.41	0.48	0.44	0.13	0.08	0.35	1.00	0.75	1.13	0.82	0.38	0.16
FB-2	0.18	0.39	0.35	0.54	0.43	0.12	0.06	0.35	1.10	0.75	1.00	0.70	0.33	0.15
FB-3	0.21	0.28	0.27	0.50	0.25	0.07	0.04	0.47	1.71	1.01	1.47	1.25	0.77	0.23
FB-4	0.25	0.47	0.44	0.62	0.43	0.10	0.06	0.57	1.46	1.10	1.76	1.38	0.71	0.30
FB-5	0.64	2.93	1.51	2.64	1.24	0.35	0.15	0.69	3.82	2.60	6.11	3.23	3.38	1.04
FB-6	0.80	5.83	3.24	2.94	1.53	0.54	0.21	0.65	3.13	2.33	5.41	3.78	1.69	0.68

Notes: PFA = peak floor acceleration associated with cabin and counterweight; * denotes that the elevator was tested in configuration C-III, otherwise the test was conducted with the elevator placed in configuration C-I; $^+$ 100 Hz and 25 Hz denote the high frequency cutoff values for the two band-pass filters.

DOI: 10.1002/eqe

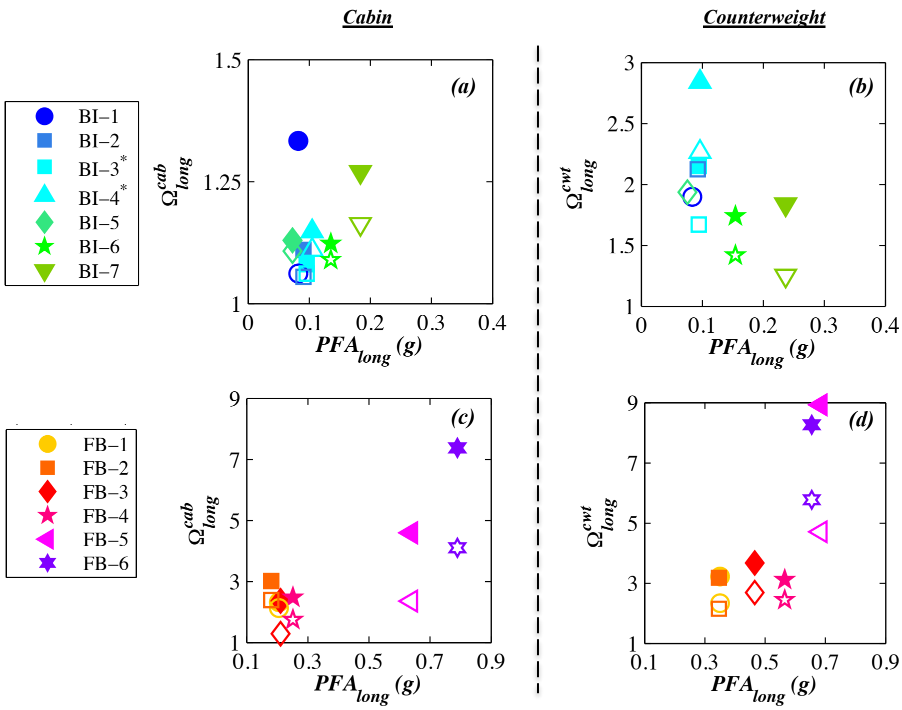

Figure 9. Acceleration amplification ratios: (a) cabin in the base isolated tests, (b) counterweight in the base isolated tests, (c) cabin in the fixed base tests, and (d) counterweight in the fixed base tests (solid markers denote the high frequency cutoff of 100 Hz, while hollow markers denote the high frequency cutoff of 25 Hz; * denotes that the elevator was tested in configuration C-III, otherwise the test was conducted with the elevator placed in configuration C-I).

5.2.2. Anchor forces. Figure 10 provides the force time histories of the bracket anchors at floor 5 (SG-E-5N/S and SG-W-5N/S) during test FB-5. To obtain the anchor forces, the strains measured from the instrumented anchors were filtered with a low-pass fourth-order Butterworth filter with a corner frequency of 15 Hz and subsequently converted to anchor forces using the calibration factors determined prior to the tests. It is noted that test FB-5 represents an earthquake scenario that achieved the design performance objectives of the building (PIDR of 2.5 % and PFA of 1.0 g). The figure demonstrates that the response characteristics of the anchor forces on the two sides of the walls differed distinctly. The peak forces were more than 7 kN on the east wall but less than 1.5 kN on the west wall, and the occurrences of these peaks at the two sides of the walls appeared to be uncorrelated. The reason for this was that the peak anchor forces of the east wall (SG-E-5S and SG-E-5N) were dominated by pounding of the counterweight with its guide-rails, while those of the west wall (SG-W-5S and SG-W-5N) were induced by multiple-support differential displacements of the cabin guide-rail supports (the cabin was located at level 1 during the fixed base tests).

Table IV presents the peak forces in the wedge anchors from the mid-height of level 4 to the mid-height of level 5 in the fixed base test phase (see Figure 10 for the anchor locations). It is noted that the forces measured on the instrumented T-headed anchor channel bolts in these tests appeared much larger than the expected values, since these bolts should have registered only insignificantly small forces (<< 1 kN) if the pretension of the bolts were properly applied. Due to the uncertainties of the pretension on these bolts during the seismic tests and the associated influences on the validity of these force measurements, the measured forces of these bolts are not presented. During the design event (FB-5) and above-design event (FB-6) tests, the anchor forces of the west wall were larger at the mid-height of level 4 than those at the higher levels. This is due to the fact that these forces were dominated by differential displacements of the guide-rails and the building PIDR demands at level

DOI: 10.1002/eqe

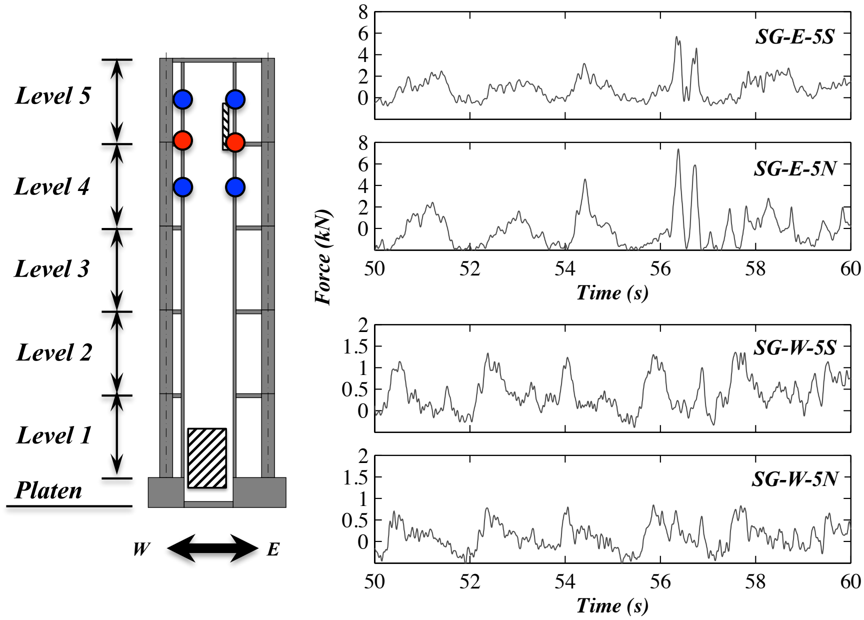

Figure 10. Time histories of the forces in the anchors supporting the brackets at floor 5 (solid red circles) during test FB-5 (solid blue circles represents the anchors supporting the brackets at mid-height level 4 and level 5, these anchor force results are later presented in Table IV).

Table IV. Peak anchor forces of the brackets from the mid-height of level 4 to the mid-height of level 5 during the fixed base tests.

Test	Anchor location	*PFA* [1]	*PIDR* [2]	West wall		East wall	
				South	North	South	North
		(g)	(%)	(kN)	(kN)	(kN)	(kN)
FB-1	Mid-height level 5	–	0.13	– [3]	0.9	1.2	2.5
	Floor 5	0.35	–	0.4	0.4	3.7	2.7
	Mid-height level 4	–	0.24	0.6	0.7	1.1	0.8
FB-2	Mid-height level 5	–	0.14	–	1.1	0.9	3.1
	Floor 5	0.39	–	0.5	0.4	3.0	1.5
	Mid-height level 4	–	0.26	0.7	0.8	1.2	0.6
FB-3	Mid-height level 5	–	0.23	–	1.2	1.6	4.6
	Floor 5	0.58	–	0.5	0.5	4.5	3.4
	Mid-height level 4	–	0.43	1.1	1.3	1.6	1.4
FB-4	Mid-height level 5	–	0.36	–	1.6	2.3	4.3
	Floor 5	0.64	–	0.9	0.9	4.8	4.6
	Mid-height level 4	–	0.74	1.0	1.0	3.9	3.2
FB-5	Mid-height level 5	–	0.54	–	2.1	5.0	9.4
	Floor 5	0.99	–	1.4	1.0	5.7	7.4
	Mid-height level 4	–	1.09	2.8	3.1	6.2	5.9
FB-6	Mid-height level 5	–	0.66	–	2.3	6.5	10.0
	Floor 5	0.90	–	1.4	1.1	4.9	8.4
	Mid-height level 4	–	1.29	6.4	7.7	6.8	7.7

[1] *PFA* = peak floor acceleration at floor 5; [2] *PIDR* = peak interstory drift ratio at levels 4 and 5; [3] the embedded strain gage in the anchor was damaged prior to the seismic tests.

4 were consistently larger compared to those at level 5 during the fixed base tests (see Figure 3(b)). In contrast, the anchor forces of the east wall were larger at floor 5 and mid-height level 5, since these anchors were attached to the brackets that were closer to the location of impact between the counterweight and the guide-rails. These forces were as large as 10 kN with PFAs at floor 5 of about 1.0 g during the last two FB tests, while those of the west wall achieved the largest values of about 3 kN in FB-5 with an associated PIDR of 1.09 % and 8 kN in FB-6 with an associated PIDR of 1.29 %. The comparison of the anchor forces on the two sides of the walls indicates that the anchor forces due to differential displacement (on the west wall) were comparable to those induced by the seismic impact between the counterweight and the guide-rails (on the east wall) during an design-level earthquake. It is noted that the controlling nominal tensile strength of the wedge anchors was 31.8 kN per ACI 318-14 [25]. Since the maximum seismic force on the wedge anchors attained during the earthquake tests was only 10 kN, these anchors had a safety factor of about 3 even for the above-design event (FB-6).

6. CONCLUSIONS

A fully functional elevator was installed within a full-scale five-story reinforced concrete building and was subsequently tested with the building under a range of earthquake motions with increasing intensity. In addition, low-amplitude white noise base excitation tests were conducted to study the dynamic response of the elevator while the locations of the cabin and counterweight were varied. Important findings regarding the dynamic characteristics and seismic behavior of the elevator system in these shake table tests as well as their implications related to seismic design of elevator systems are summarized as follows:

1. Low-amplitude white noise base excitation tests indicate that the acceleration amplification effect of the counterweight was larger than that of the cabin when their vertical locations were comparable. While the amplification ratios of both the cabin and the counterweight were as large as 5 when they were at the top of the building (level 5), the counterweight observed much higher amplification ratios (twice as high as those of the cabin) when placed at the middle (level 3) and the bottom (level 1) of the building. This may be attributed to their varying attachment details, guide-rail flexibility, and gap provisions related to the guide-rails.
2. The elevator remained functioning up to and including the design event earthquake. Major damage to the elevator system was restricted to the entrance doors when the interstory drift demands were more than twice as large as the design recommended values (2.5 % interstory drift). The extremely large interstory drift demands at the lower three levels of the test building (6 % interstory drift) caused severe distortion and corner crushing of the elevator doors as a result of significant interaction between the doors and their surrounding cold-formed steel partition walls. Damage to the doors resulted in impaired elevator functionality and safe egress as well as loss of compartmentation in the case of post-earthquake fire.
3. Seismic impact between the elevator components (cabin and counterweight) and the guide-rails produced high-amplitude impulse-like accelerations (as large as 6 g) on these components during the design and above-design events (FB-5 and FB-6). The corresponding peak accelerations of these components were significantly reduced (about 1.5 g for the cabin and 3 g for the counterweight) when the impact-induced acceleration spikes were removed using a low pass filter, however these measured acceleration demands remain well above the ASME A17.1 design recommendation value (0.5 g).
4. While the elevator components (cabin and counterweight) observed moderate amplification effects during the first four FB tests (Ω attaining as large as 3 for the cabin and 4 for the counterweight), the observed acceleration amplification ratios of these components increased significantly during the last two FB tests (Ω attaining as large as 7 for the cabin and 9 for the counterweight). These values are much larger than that suggested by ASCE 7 provisions for elevator components, in which they are assumed as rigid components with a component amplification factor of 1.0. Future investigations are needed to provide

DOI: 10.1002/eqe

understanding regarding expected peak accelerations of elevator components during service, design, and maximum considered earthquakes.

5. Differential displacements of the bracket supports may impose considerable forces on the guide-rails and may result in plastic yielding of guide-rails. With a PFA of 0.9 g at floor 5 and a PIDR of 1.3 % at level 4 during the last FB test (FB-6), the peak anchor forces induced by differential displacements on the west wall (~8 kN) were comparable with those induced by the impact between the elevator components and the guide-rails on the east wall (~10 kN). Therefore, it is recommended that the effects of differential displacements be considered in the design of elevator guide-rails.

These system-level shake table tests allowed investigation of the seismic behavior of an elevator system as installed within a full-scale building when subjected to realistic dynamic loading. A complete set of high-quality test data of the elevator system in these shake table tests is publicly available [26, 27]. These results may provide useful input for calibration of computational tools as well as future design codes for elevator systems. Importantly, these tests highlight the necessity for addressing the interaction of elevator doors with their surrounding components in future design to improve the seismic resilience of elevator systems. In addition, the use of well-restrained guide shoes with air gaps is recommended as it demonstrated the potential of effectively reducing the derailment hazard of cabins and counterweights during high-intensity earthquakes.

ACKNOWLEDGEMENTS

This project is a collaboration between four academic institutions (University of California, San Diego, San Diego State University, Howard University, and Worcester Polytechnic Institute), four government or other granting agencies (the National Science Foundation, the Englekirk Advisory Board, the Charles Pankow Foundation, and the California Seismic Safety Commission), over 40 industry partners, and two oversight committees (http://bncs.ucsd.edu). Through the NSF-NEESR program, partial funding is provided by grant number CMMI-0936505. Support is also provided by NEES@UCSD and NEES@UCLA staff, Robert Bachman, Dr. Robert Englekirk, Mahmoud Faghihi, Dr. Philipp Grosser, Jahida Nadi, John Silva, and Prof. Ken Walsh. This work would not be possible without the many hours of dedicated graduate student contributions, in particular, Consuelo Aranda, Michelle Chen, Hamed Ebrahimian, Elias Espino, Giovanni De Francesco, Jin-Kyung Kim, Steven Mintz (deceased), Yoshua Neuman, Elide Pantoli, Hae-Jun Park, and Francesco Selva. Specific to the elevator discussed in this paper, the authors appreciate the support of Schindler Elevator Corporation for providing the elevator and Hilti Corporation for supporting its anchor installations. The above continuous support is gratefully acknowledged. Opinions and findings of this study are of the authors and do not necessarily reflect those of the sponsors.

REFERENCES

1. International Code Council. *International Building Code*. International Code Council: Falls Church, VA, 2012.
2. Federal Emergency Management Agency. *Reducing the risks of nonstructural earthquake damage - a practical guide*. Federal Emergency Management Agency: Washington, D.C., 2014.
3. ASME A171. *Safety Code for Elevators and Escalators*. American Society of Mechanical Engineers: New york, NY, 2010.
4. Schiff A. The Whittier Narrows, California earthquake of October 1, 1987-response of elevators. *Earthquake Spectra* 1988; **4**(2):367–375.
5. Suárez LE, Singh MP. Review of earthquake performance, seismic codes, and dynamic analysis of elevators. *Earthquake spectra* 2000; **16**(4):853–878.
6. Mitrani-Reiser J, Mahoney M, Holmes WT, de la Llera JC, Bissell R, Kirsch T. A functional loss assessment of a hospital system in the bío-bío province. *Earthquake Spectra* 2012; **28**(S1):S473–S502.
7. EERI. M 6.0 south Napa earthquake of August 24, 2014. *EERI Special Earthquake Report – October 2014*, Earthquake Engineering Research Institue, Oakland, CA 2014.
8. Yang T, Kullegowda H, Kapania RK, Schiff AJ. Dynamic response analysis of elevator model. *Journal of Structural Engineering* 1983; **109**(5):1194–1210.
9. Tzou H, Schiff A. Structural dynamics of elevator counterweight systems and evaluation of passive constraint. *Journal of Structural Engineering* 1988; **114**(4):783–803.
10. Segal F, Rutenberg A, Levy R. Earthquake response of structure-elevator system. *Journal of structural engineering* 1996; **122**(6):607–616.
11. Singh MP, Suarez LE, Rildova. Seismic response of rail-counterweight systems in elevators. *Earthquake Engineering and Structural Dynamics* 2002; **31**(2):281–303.
12. Singh MP, Rildova, Suarez LE. Non-linear seismic response of the rail-counterweight system in elevators in buildings. *Earthquake Engineering and Structural Dynamics* 2004; **33**(2):249–270.

13. Yao G, Tseng C, Shen T. Elevator CW derailment research in Taiwan. *Proc. of the 13th World Conference on Earthquake Engineering*, Vancouver, B.C., Canada, Aug 1-6, 2004.
14. Van Den Einde L, Restrepo JI, Conte J, Luco E, Seible F, Filiatrault A, Clark A, Johnson A, Gram M, Kusner D, *et al.*. Development of the George E. Brown Jr. network for earthquake engineering simulation (NEES) large high performance outdoor shake table at the University of California, San Diego. *Proc. of the 13th World Conference on Earthquake Engineering*, Vancouver, B.C., Canada, Aug 1-6, 2004.
15. Chen M, Pantoli E, Wang X, Astroza R, Ebrahimian H, Mintz S, Hutchinson T, Conte J, Restrepo J, Meacham B, *et al.*. BNCS Report #1: Full-scale structural and nonstructural building system performance during earthquakes and post-earthquake fire – specimen design, construction, and test protocol. *SSRP-2013/09*, Department of Structural Engineering, University of California, San Diego, La Jolla, CA 2013.
16. Chen MC, Pantoli E, Wang X, Astroza R, Ebrahimian H, Hutchinson TC, Conte JP, Restrepo JI, Marin C, Walsh KD. Full-scale structural and nonstructural building system performance during earthquakes: Part I – Specimen description, test protocol and structural response. *Earthquake Spectra.* 2015; In press.
17. Pantoli E, Chen MC, Wang X, Astroza R, Ebrahimian H, Hutchinson TC, Conte JP, Restrepo JI, Marin C, Walsh KD, *et al.*. Full-scale structural and nonstructural building system performance during earthquakes: Part II – NCS damage states. *Earthquake Spectra* 2015; In press.
18. Wang X, Pantoli E, Hutchinson C, Restrepo J, Wood R, Hoehler M, Grzesik P, Sesma F. Seismic performance of cold-formed steel wall systems in a full-scale building. *Journal of Structural Engineering* ; doi:10.1061/(ASCE)ST. 1943-541X.0001245.
19. Pantoli E, Chen M, Wang X, Astroza R, Ebrahimian H, Mintz S, Hutchinson T, Conte J, Restrepo J, Meacham B, *et al.*. BNCS Report #2: Full-scale structural and nonstructural building system performance during earthquakes and post-earthquake fire – test results. *SSRP-2013/10*, Department of Structural Engineering, University of California, San Diego, La Jolla, CA 2013.
20. Skolnik DA, Wallace JW. Critical assessment of interstory drift measurements. *Journal of structural engineering* 2010; **136**(12):1574–1584.
21. Pantoli E, Chen M, Hutchinson T, Restrepo J. BNCS Report #3: Full-scale structural and nonstructural building system performance during earthquakes and post-earthquake fire – camera and analog sensor details. *SSRP-2013/11*, Department of Structural Engineering, University of California, San Diego, La Jolla, CA 2013.
22. Astroza R, Ebrahimian H, Conte J, Restrepo J, Hutchinson T. System identification of a full-scale five-story reinforced concrete building tested on the nees-ucsd shake table. *Structural Control and Health Monitoring* ; In press.
23. Meacham BJ. Post-earthquake fire performance of buildings: Summary of a large-scale experiment and conceptual framework for integrated performance-based seismic and fire design. *Fire Technology* 2015; :1–25.
24. ASCE 7-10. *Minimum design loads for buildings and other structures*. American Society of Civil Engineers: Reston, VA, 2010.
25. American Concrete Institute (ACI). *Building Code Requirements for Structural Concrete and Commentary*. American Concrete Institute: Farmington Hills, MI, 2014.
26. Hutchinson T, Restrepo J, Conte J, Pantoli E, Chen M, Wang X, Astroza R, Ebrahimian H. Shake table testing of a five story building outfitted with NCSs (BNCS project) 2014; doi:10.4231/D38W38349.
27. Pantoli E, Chen MC, Hutchinson TC, Astroza R, Conte J, Ebrahimian H, Restrepo J, Wang X. Landmark dataset from the building nonstructural components and systems (BNCS) project. *Earthquake Spectra* 2015; In press.